The Electrical Asymmetry Effect - A novel and simple method for separate control of ion energy and flux in capacitively coupled RF discharges

2009 J. Phys.: Conf. Ser. 162 012010

(http://iopscience.iop.org/1742-6596/162/1/012010)

Journal of Physics: Conference Series **162** (2009) 012010 doi:10.1088/1742-6596/162/1/012010

The Electrical Asymmetry Effect - A novel and simple method for separate control of ion energy and flux in capacitively coupled RF discharges

U. Czarnetzki[1], B. G. Heil[1,4], J. Schulze[1], Z. Donkó[2], T. Mussenbrock[3], and R. P. Brinkmann[3]

[1]Institute for Plasma and Atomic Physics, Ruhr-University Bochum, Germany
[2]Research Institute for Solid State Physics and Optics of the Hungarian Academy of Science, Budapest, Hungary
[3]Institute for Theoretical Electrical Engineering, Ruhr-University Bochum, Germany
[4]Current address: Richardt Patents & Trademarks, Leergasse 11, D-65343 Eltville am Rhein, Germany

E-mail: fjschulze@hotmail.com

Abstract.

If a temporally symmetric voltage waveform is applied to a capacitively coupled radio frequency (CCRF) discharge, that contains one or more even harmonics of the fundamental frequency, the sheaths in front of the two electrodes will necessarily be asymmetric even in a geometrically symmetric discharge. Optimally this is achieved with a dual-frequency discharge driven at a phase locked fundamental frequency and its second harmonic, e.g. 13.56 MHz and 27.12 MHz. An analytical model, a hybrid fluid/Monte-Carlo kinetic model as well as a Particle in Cell (PIC) simulation show that this Electrical Asymmetry Effect (EAE) leads to the generation of a DC self bias as a function of the phase between the applied voltage harmonics in geometrically symmetric as well as asymmetric discharges. The DC self bias depends almost linearly on the phase angle and the role of the electrodes (powered and grounded) can be reversed. At low pressures the EAE is self-amplifying due to the conservation of ion flux in the sheaths. By tuning the phase, precise and convenient control of the ion energy at the electrodes can be achieved, while the ion flux remains constant. The maximum ion energy can typically be changed by a factor of about three at both electrodes. At the same time the ion flux is constant within $\pm 5\%$.

1. Introduction

Capacitively coupled radio frequency (CCRF) discharges play an important role for industrial applications such as etching and deposition processes for semiconductor fabrication (chip production, solar cells, etc.). In this context separate control of the ion flux and the ion energy at the substrate surface is essential. The ion energy controls the individual processes taking place at the wafer surface and the ion flux determines the throughput of a given process [1].

Separate control of ion flux and ion energy cannot be achieved in conventional single frequency discharges, since both parameters are controlled by the applied voltage amplitude [2]-[33]. Besides hybrid discharges [34] the usual method to solve this problem is the use of dual-frequency CCRF discharges operated at two substantially different frequencies, typically 2 MHz and 27 MHz, applied to one or more electrodes [20],[35]-[46]. Usually the low frequency voltage is much higher than the high frequency voltage. The ion energy is mainly controlled by the low frequency component. The ion flux is mainly controlled by the high frequency component, since electron heating is more efficient at higher frequencies. However, recent investigations have shown, that there can be a strong coupling between the two frequencies, that might limit separate control of ion flux and energy [20], [40]-[45].

Here we propose a completely novel method to achieve separate control of ion energy and flux at the electrode surfaces in a simple and almost ideal way in dual-frequency CCRF discharges operated at similar frequencies, namely 13.56 MHz and 27.12 MHz [47, 48, 49]. If one electrode is driven at a fundamental frequency and its second harmonic with variable phase between the two voltage waveforms, a DC self (electrical asymmetry) bias will develop as a function of the phase angle even in a geometrically symmetric CCRF discharge. This variable DC self bias controls the ion energy at the electrodes. Therefore, by adjusting the phase the ion energy can be controlled. As only the relative phase between the voltage harmonics and not their amplitude is changed, the ion flux at the electrodes remains constant.

This Electrical Asymmetry Effect (EAE) is investigated here in three different ways: An analytical proof and model, a hybrid hydrodynamic and Monte-Carlo kinetic model [47, 48, 50], and a self consistent particle-in-cell simulation (PIC) [49]. All three models yield very similar results with the PIC simulation revealing further insight into kinetic details. The paper is structured in the following way: In section 2 it will be demonstrated that the sheaths in a CCRF discharge operated at a fundamental frequency and one or more even harmonic are necessarily asymmetric. In section 3 the analytical model to describe the EAE is presented and the results are compared to a hybrid hydrodynamic and Monte-Carlo kinetic model. In section 4 the results of a self-consistent PIC simulation are presented and separate control of ion energy and flux via the EAE is demonstrated. In section 5 conclusions are drawn.

2. Electrical Asymmetry in CCRF discharges driven at a fundamental frequency and one or more even harmonics

The two sheaths in a CCRF discharge are symmetric only if the following condition holds [47, 48]:

$$V_{sp}(\omega t) = -V_{sg}(\omega t + \pi) \tag{1}$$

where V_{sp} and V_{sg} are the voltage drops across the sheath at the powered and grounded electrode, respectively. The voltage drop across the discharge, V_{tot}, is assumed to be the sum of both sheath voltages. This assumption is verified by the PIC simulation [49].

$$V_{tot} = V_{sp} + V_{sg} \tag{2}$$

V_{tot}, V_{sp}, and V_{sg} can be decomposed into their Fourier components:

$$V_{tot} = \sum_{n=-N}^{N} t_n e^{in\omega t} \tag{3}$$

$$V_{sp} = \sum_{n=-\infty}^{\infty} p_n e^{in\omega t} \tag{4}$$

$$V_{sg} = \sum_{n=-\infty}^{\infty} g_n e^{in\omega t} \tag{5}$$

Equations 2 through 5 imply that:

$$t_n = p_n + g_n \quad \forall \quad |n| \leq N \tag{6}$$

$$0 = p_n + g_n \quad \forall \quad |n| \geq N \tag{7}$$

Substituting equations 4 and 5 into the criterion for symmetric sheaths (equation 1) yields:

$$\sum_{n=-\infty}^{\infty} p_n e^{in\omega t} = -\sum_{n=-\infty}^{\infty} g_n e^{in(\omega t+\pi)} \tag{8}$$

This implies that the sheaths are only electrically symmetric if:

$$p_n = -g_n e^{in\pi} \tag{9}$$

$e^{in\pi} = 1$ whenever n is even and $e^{in\pi} = -1$ whenever n is odd. Using equations 9 and 6 yields:

$$t_n = \begin{cases} 0 & \forall \quad n = 0, 2, 4, 6, ... \\ 2p_n & \forall \quad n = 1, 3, 5, 7, ... \end{cases} \tag{10}$$

Based on equation 10 it is clear that the amplitudes of the fundamental and any odd harmonic can be freely chosen in order to obtain electrically symmetric sheath. However, there must not be any even voltage harmonic. If there is an even harmonic, the sheaths will necessarily be electrically asymmetric.

3. Modeling of the EAE

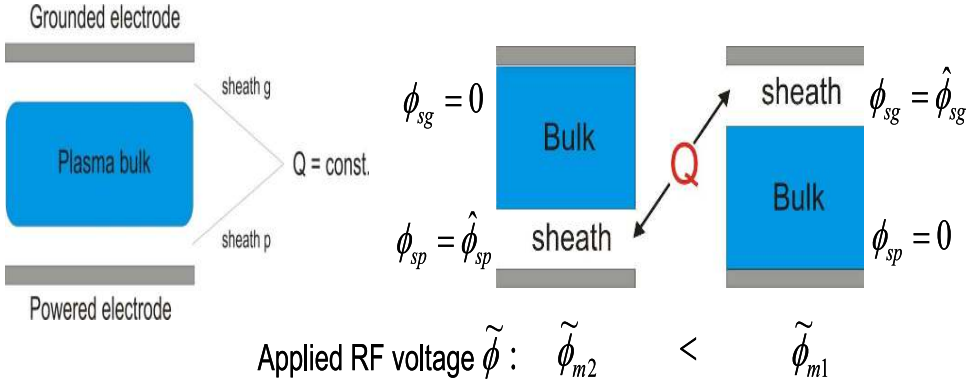

Figure 1. Sketch of a CCRF discharge (left) and location of the net positive charge in the discharge Q at the phase of complete sheath collapse at the grounded (middle) and powered electrode (right). ϕ_{sp} and ϕ_{sg} are the sheath voltages at the powered and grounded electrode, respectively. $\hat{\phi}_{sp}$, $\hat{\phi}_{sg}$ are the maxima of the sheath voltages. $\tilde{\phi}$ is the applied RF voltage and $\tilde{\phi}_{m1}$, $\tilde{\phi}_{m2}$ are the maximum and minimum of the applied voltage waveform, respectively.

Figure 1 shows the typical setup of a CCRF discharge of two plane parallel electrodes, one powered and one grounded, of either the same (geometrically symmetric) or different (geometrically asymmetric) surface areas. The discharge consists of a quasineutral plasma bulk and two sheaths adjacent to each electrode. The net positive charge in the entire discharge Q is located in the sheaths. Here Q is assumed to be constant within one RF period, which has been demonstrated to be a good approximation [16]. The voltage balance for such a CCRF discharge is:

$$\tilde{\phi} + \eta = \phi_{sp} + \phi_{sg} \tag{11}$$

where $\tilde{\phi}$ is the applied RF voltage, η the DC self-bias and ϕ_{sp}, ϕ_{sg} are the sheath voltages at the powered and grounded electrode, respectively. Here the floating potential and the voltage drop across the bulk are neglected and the voltage drop across the discharge is assumed to be determined only by the sum of both sheath voltages. A PIC simulation has demonstrated that this assumption is justified [49]. At two distinct phases within one RF period one sheath is completely collapsed at one of the electrodes (see figure 1). If the sheath is collapsed at the grounded electrode, the applied RF voltage $\tilde{\phi}$ will be minimum ($\tilde{\phi} = \tilde{\phi}_{m2}$), no voltage will drop across the sheath at ground ($\phi_{sg} = 0$) and maximum voltage will drop across the sheath at the powered electrode ($\phi_{sp} = \hat{\phi}_{sp}$). Vice versa if the sheath is collapsed at the powered electrode, the applied RF voltage will be maximum ($\tilde{\phi} = \tilde{\phi}_{m1}$), no voltage will drop across the sheath at the powered electrode ($\phi_{sp} = 0$) and maximum voltage will drop across the sheath at ground ($\phi_{sg} = \hat{\phi}_{sg}$). The voltage balance of equation 11 at these two distinct phases is given by:

$$\tilde{\phi}_{m2} + \eta = \hat{\phi}_{sp} \tag{12}$$

$$\tilde{\phi}_{m1} + \eta = \hat{\phi}_{sg} \tag{13}$$

The maximum sheath voltages $\hat{\phi}_{sp}$ and $\hat{\phi}_{sg}$ can be calculated by integrating Poisson's equation at the corresponding phase:

$$\hat{\phi}_{sp} = -\frac{1}{2e\varepsilon_0}\left(\frac{Q_{mp}}{A_p}\right)^2 \frac{I_{sp}}{\bar{n}_{sp}} \tag{14}$$

$$\hat{\phi}_{sg} = -\frac{1}{2e\varepsilon_0}\left(\frac{Q_{mg}}{A_g}\right)^2 \frac{I_{sg}}{\bar{n}_{sg}} \tag{15}$$

Here e is the elementary charge, ε_0 the dielectric constant, $Q_{mp,mg}$ the maximum charge in the sheath at the powered and grounded electrode, respectively, $A_{p,g}$ the surface area of the respective electrode, $\bar{n}_{sp,sg}$ the mean ion density in the respective sheath and $I_{sp,sg}$ the respective sheath integral.

$$I_s = 2\int_0^1 p_s(\xi)\xi d\xi \tag{16}$$

with $\xi = x/s_m$ and $p_s(\xi) = n_{\mathrm{i}}(x)/\bar{n}_{\mathrm{i}}$. Here s_m is the maximum sheath width and n_{i} is the ion density.
Under the assumption of constant total charge Q the ratio of equations 14 and 15 yields:

$$\varepsilon = \left|\frac{\hat{\phi}_{sg}}{\hat{\phi}_{sp}}\right| = \left(\frac{A_p}{A_g}\right)^2 \frac{\bar{n}_{sp}}{\bar{n}_{sg}}\frac{I_{sg}}{I_{sp}} \tag{17}$$

ε is called the symmetry parameter [48]. Using equations 17, 12, and 13 the following expression for the DC self bias is derived, that depends only on the extremes of the applied RF voltage waveform and the symmetry parameter:

$$\eta = -\frac{\tilde{\phi}_{m1} + \varepsilon\tilde{\phi}_{m2}}{1+\varepsilon} \tag{18}$$

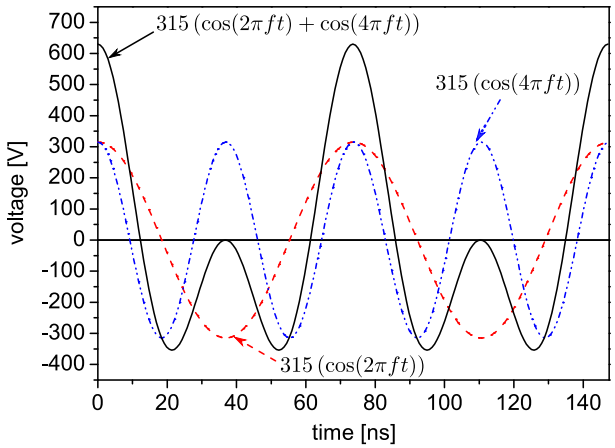

Figure 2. Voltage waveform $\tilde{\phi}(t) = 315\,(\cos(2\pi ft) + \cos(4\pi ft))$, where $f = 13.56\,\mathrm{MHz}$, applied to the discharge for two RF periods (solid black line). The absolute values of the positive and negative extremes and the voltages across the two sheaths are different. Therefore, a DC self bias develops under these conditions [49].

From now on we consider a geometrically symmetric CCRF discharge ($A_p = A_g$) in argon operated at 2.7 Pa with an electrode gap of $d = 6.7\,\mathrm{cm}$, similar to conditions of an experimental investigation by Godyak and Piejak in a single frequency CCRF discharge [18, 19, 21, 47, 50, 51]. The following RF voltage waveform is applied to one of the electrodes:

$$\tilde{\phi}(t) = 315\,\mathrm{V}\,(\cos(2\pi\mathrm{ft} + \theta) + \cos(4\pi\mathrm{ft})) \tag{19}$$

with $f = 13.56\,\mathrm{MHz}$. θ is the phase angle between the harmonics. Figure 2 shows this voltage waveform as well as the fundamental cosine function and its second harmonic for $\theta = 0°$. Each of the two cosine functions is harmonically symmetric ($\tilde{\phi}(\varphi+\pi) = -\tilde{\phi}(\varphi)$, $\varphi = \omega t$, $\tilde{\phi}$ corresponds to the applied voltage), but the sum of the two is not. The sum is symmetric with respect to $\varphi = \pi$ ($\tilde{\phi}(\varphi) = \tilde{\phi}(-\varphi)$). The absolute values of the positive and negative extremes are different. Therefore, according to equation 18 at $\theta = 0°$ a DC self bias will be generated ($\varepsilon \leq 1$).

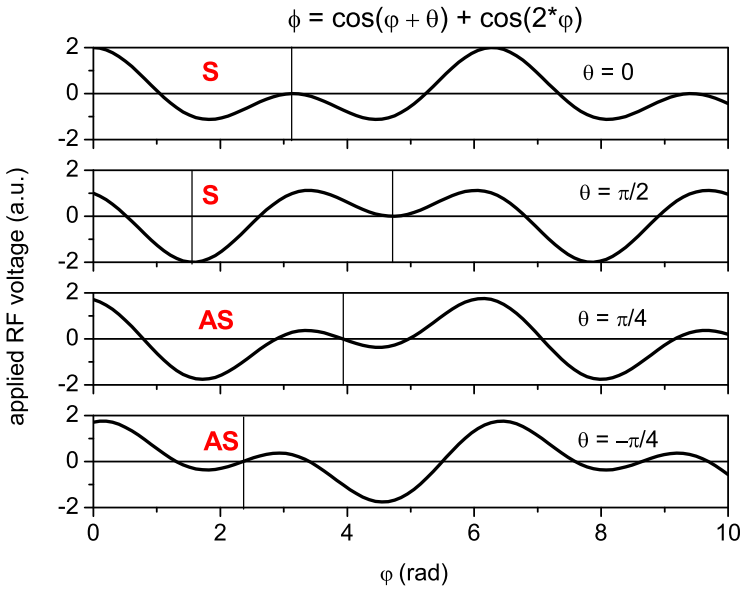

Figure 3. RF voltage waveform according to equation 19 at different phase angles θ [48].

By tuning the phase angle θ from 0° to 90° the symmetry of the applied RF voltage waveform is changed from symmetric (S, $\theta = 0°$) to anti-symmetric (AS, $-\tilde{\phi}(\varphi) = \tilde{\phi}(-\varphi)$, $\theta = 45°$) and back to symmetric (S, $\theta = 90°$). This is shown in figure 3. In case of an anti-symmetric waveform the absolute values of the positive and negative extremes are the same and no DC self bias will develop. At $\theta = 90°$, $\eta_{(90°)} = -\eta_{(0°)}$. Already based on this simple graphical analysis it is obvious that by adjusting the phase between the applied voltage harmonics the DC self bias can be changed (assuming $\varepsilon = 1$).

In order to calculate η explicitly ε needs to be known. ε is calculated by using the charged particle densities resulting from the Brinkmann sheath model [52, 53]. Then equation 19 is solved for its extrema $\tilde{\phi}_{m1}$ and $\tilde{\phi}_{m2}$. Using equation 18 this procedure yields the DC self bias at different phase angles θ.

Figure 4 shows the symmetry parameter resulting from the Brinkmann sheath model and a PIC simulation, that will be discussed in detail later. Obviously, the symmetry parameter changes with the phase from $\theta = 0°$ to $\theta = 90°$. At low pressures the sheath is collisionless and a finite DC self bias leads to different mean sheath voltages. Due to flux continuity different mean sheath voltages lead to different mean ion densities in both sheaths. This causes ε to deviate from unity. According to equation 18 such a dependence of ε on the phase leads to a self-amplifications of the EAE [48].

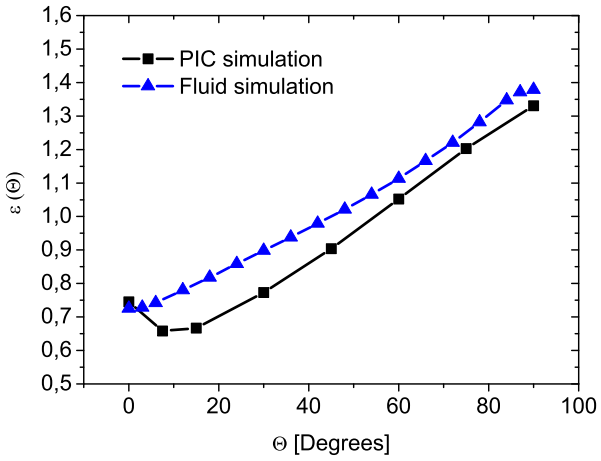

Figure 4. Symmetry parameter defined by equation 17 as a function of the phase angle θ (blue line (triangles) - fluid simulation [48], black line (squares) - PIC simulation) [49].

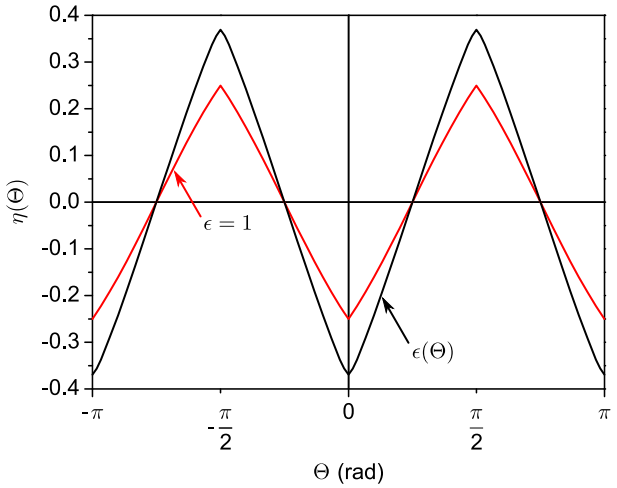

Figure 5. Normalized DC self bias as a function of the phase between the applied voltage harmonics resulting from equation 18 using $\varepsilon = 1$ and ε resulting from the Brinkmann sheath model (figure 4) [48].

Figure 5 shows the normalized DC self bias as a function of the phase between the applied voltage harmonics resulting from equation 18 using $\varepsilon = 1$ and $\varepsilon(\theta)$ resulting from the Brinkmann sheath model (figure 4). The self-amplification is obvious.

The Brinkmann sheath model can also be used to directly calculate the DC self bias. Figure 6 shows a comparison between η resulting from the analytical model, the Brinkmann sheath model, and a PIC simulation. All approaches yield similar results. The DC self bias is an almost linear function of θ.

Similar to the way the maximum sheath voltages were calculated (equations 14,15) the sheath voltages can also be calculated as a function of time within one RF period by using the temporary sheath edge instead of the maximum for the integration of Poisson's equation. Figure 7 shows the resulting sheath voltages as a function of the phase within one low frequency RF period.

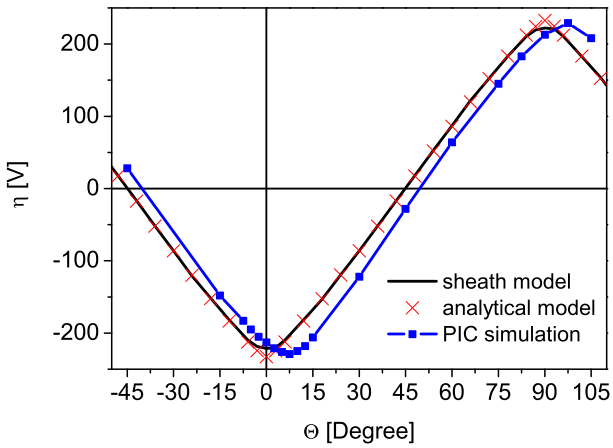

Figure 6. DC self bias η calculated by the analytical model using ε from the Brinkmann sheath model (red markers, [48]), directly by the Brinkmann sheath model (solid black line, [48]), and by a PIC simulation (blue markers and solid line) [49].

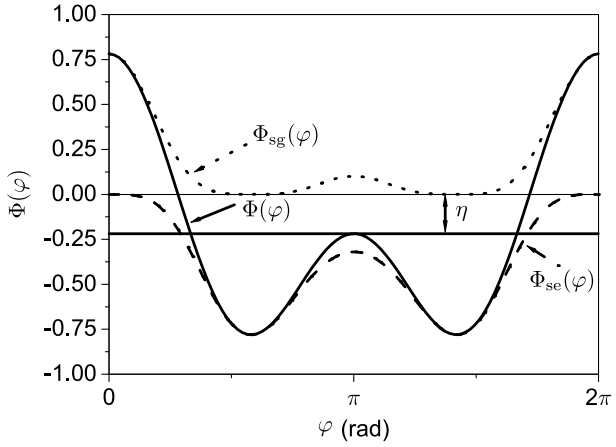

Figure 7. Sheath voltages as a function of the phase within one low frequency RF period resulting from the analytical model. The total voltage drop across the discharge and the DC self bias are also shown [48].

Similar results are also obtained from the Brinkmann sheath model.

The partial derivative of the sheath voltage ϕ_s with respect to the charge in the sheath q is given by [48]:

$$\frac{\partial \phi_s}{\partial q^2} = -\frac{1}{2e\varepsilon_0 \bar{n}(s) A^2} \tag{20}$$

Here $\bar{n}(s)$ is the average ion density in the sheath depending on the position of the sheath edge s, A is the electrode surface area. Equation 20 corresponds to a quadratic charge-voltage relation. The left plot in figure 8 shows the charge voltage relation resulting from the Brinkmann sheath model (solid line) at $\theta = 0°$ for the geometrically symmetric discharge discussed here. To a good approximation it agrees with a quadratic relation (dashed line). Such a quadratic charge voltage relation has been assumed for capacitive discharges before [13] and has been

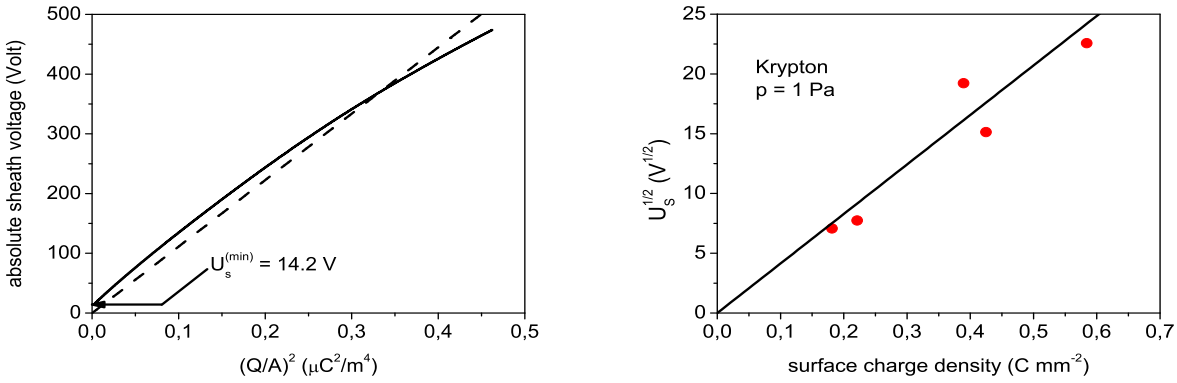

Figure 8. Left: Charge voltage relation resulting from the Brinkmann sheath model (solid line) at $\theta = 0°$ for the geometrically symmetric discharge discussed here. The simple quadratic relation is also shown (dashed line) [48]. Right: Measured charge voltage relation in a geometrically strongly asymmetric single frequency CCRF discharges operated at 13.56 MHz, 1 Pa in krypton [19, 21].

measured by Fluorescence Dip Spectroscopy in krypton in a single frequency geometrically strongly asymmetric CCRF discharge before [19, 21]. Slight deviations from an exactly quadratic relation are caused by the actual density profile in the sheath. At large sheath width $\bar{n}(s)$ in equation 20 is larger than at small sheath width.

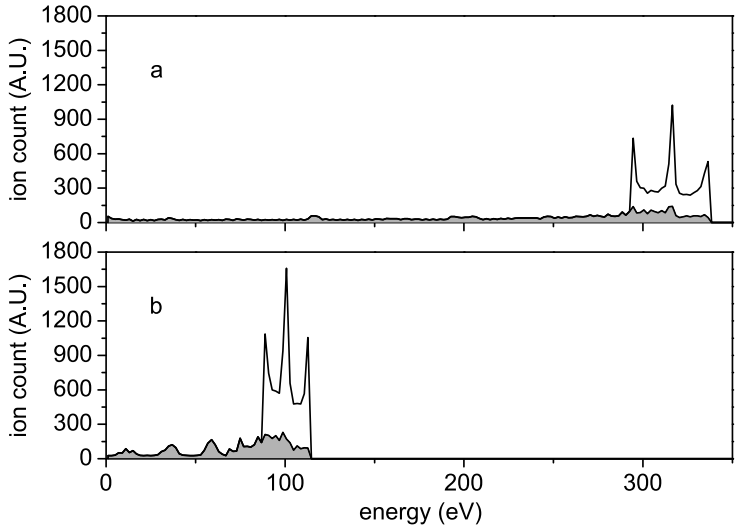

Figure 9. Ion energy distribution functions at the powered electrode at (a) $\theta = 0°$ and (b) $\theta = 90°$. The shaded regions correspond to ions that undergo a charge exchange collision [48].

The variable DC self bias (see figure 6) allows convenient and simple control of the ion energy distribution function (IEDF) at both electrodes. Here an ion Monte Carlo simulation coupled to the Brinkmann sheath model is used to calculate the IEDFs at the electrodes as a function of the phase between the applied voltage harmonics. Figure 9 shows the IEDF at the powered electrode for different phase angle θ. At $\theta = 0°$ (a) the bias is strongly negative and the mean sheath

voltage at the powered electrode is high. Therefore, the IEDF is shifted to higher energies. At $\theta = 90^\circ$ (b) the bias is strongly positive and the mean sheath voltage at the powered electrode is low. Therefore, the IEDF is shifted to lower energies.

4. PIC simulation of the EAE

Here we describe a geometrically symmetric dual-frequency CCRF discharge in argon using a one-dimensional (1d3v) bounded plasma particle-in-cell simulation code, complemented with a Monte Carlo treatment of collision processes (PIC/MCC, [20, 54, 55]). The electrodes are assumed to be infinite, planar and parallel. In our implementation of the PIC simulation, one of the electrodes is driven by a voltage specified by equation 19, while the other electrode is grounded. The electron impact cross sections for the collision processes are taken from [56]. For the positive ions, elastic collisions with the gas atoms are divided into an isotropic and a backward part [57]. The cross sections for these collisions are taken from [57, 58]. Metastable atoms are not taken into account. The bias voltage η is determined in the simulation in an iterative way to ensure that the charged particle fluxes to the two electrodes averaged over one low frequency RF period become equal. Electrons are reflected from the electrode surfaces with a probability of 0.2 and the secondary electron emission coefficient is taken to be $\gamma = 0.1$ for most of our simulations. The number of superparticles in the simulations is of the order of 10^5. From the trajectories of the particles followed in the PIC simulation as well as from the collision events we derive the spatio-temporal distributions of several plasma parameters.

The DC self bias and the symmetry parameter resulting from the PIC simulation at 2.7 Pa and an electrode gap of 6.7 cm have already been shown in figures 6 and 4, respectively. Both show good agreement with previously performed model results.

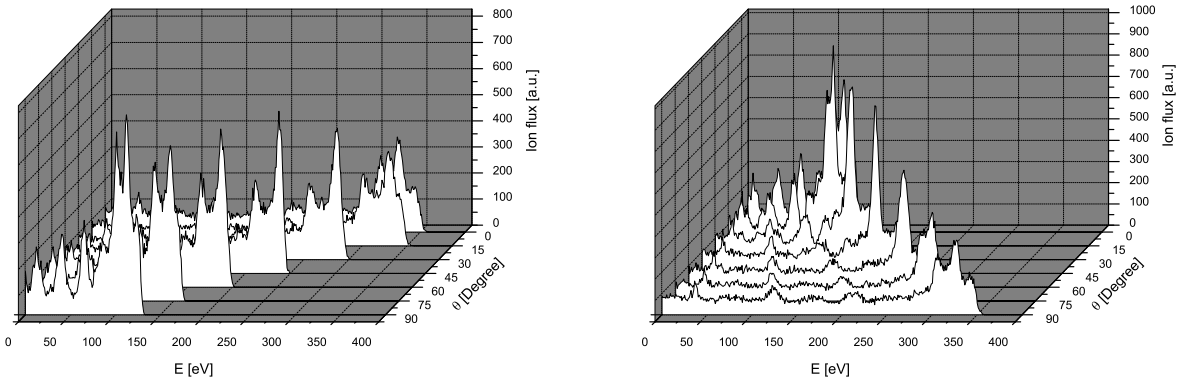

Figure 10. Ion flux-energy distributions at the powered (left) and grounded (right) electrode as a function of the phase angle θ of equation 19 calculated by the PIC simulation under the conditions mentioned in the text [49].

Figure 10 shows the ion flux-energy distribution at each electrode as a function of θ resulting from the PIC simulation. By changing θ from 0° to 90° the maximum ion energy at each electrode can be changed by a factor of about three. Furthermore, the role of each electrode can be reversed electrically. Figure 10 agrees well with the distribution functions calculated in the frame of the fluid/Monte Carlo model (see figure 9). The local maxima of the distribution functions at low energies are again caused by ions, that undergo charge exchange collisions in the sheath.

The analytical and the fluid/Monte Carlo model presented in the previous section are both not self consistent. In both models the mean plasma density is an input parameter and is not calculated self-consistently. Therefore, separate control of ion energy and flux cannot be investigated using these models. However, the PIC simulation calculates the plasma density and the ion flux self-consistently and can, therefore, be used to investigate this separate control.

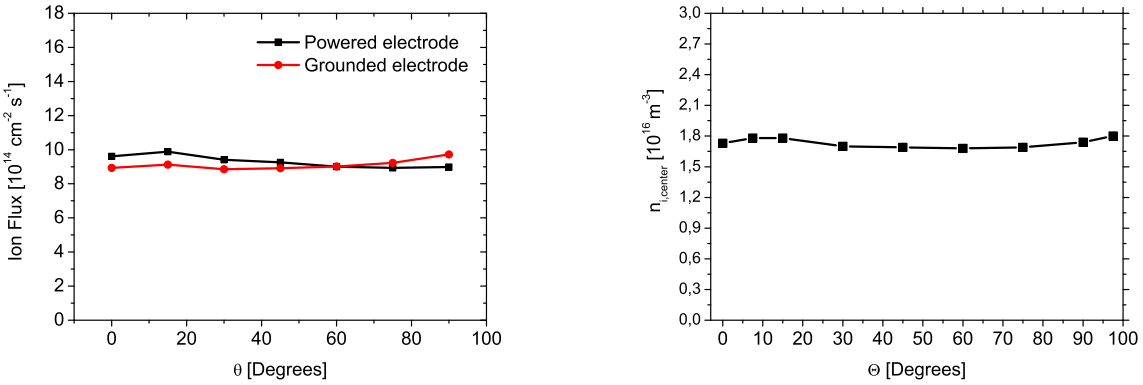

Figure 11. Left: Ion fluxes at the powered and grounded electrode as a function of the phase angle θ in equation 19 calculated by the PIC simulation [49]. Right: Ion density in the discharge center as a function of the phase angle θ (PIC) [49].

The left plot of figure 11 shows the ion flux resulting from the PIC simulation at both electrodes as the phase angle θ is varied from 0° to 90°. The ion flux is constant within $\pm 5\%$, while the maximum ion energy changes by a factor of three as θ changes (see figure 10). The observed stability of the ion flux is within the range of tolerance for most industrial applications [59, 60]. The right plot of figure 11 shows the ion density in the discharge center calculated by the PIC simulation. The ion density is basically constant as the phase angle changes. Based on the above results the EAE easily allows separate control of ion energy and ion flux by keeping the applied voltage constant and changing the phase angle θ.

In the analytical model the total voltage across the discharge is assumed to be the sum of the voltages across both sheaths (equation 2). Generally, the total voltage across the discharge is the sum of the applied voltage, V_{AC}, and the DC self bias, η:

$$V_{total} = \tilde{\phi} + \eta \tag{21}$$

The PIC simulation shows that the assumption corresponding to equation 2 is correct under the conditions investigated here: At the low pressure of 20 mTorr, the voltage drop across the plasma bulk is negligible and the total voltage across the discharge is indeed the sum of both sheath voltages.

For the PIC simulation the voltage is an input parameter and the voltage amplitude is kept constant. However, in experiments the applied power and not the voltage is usually set externally. Therefore, it is important to examine how the absorbed power changes as a function of θ while the voltage amplitude is kept constant. The mean power density absorbed by electrons and ions, $\bar{p}_{\mathrm{e,i}}$, results from an integration of the space and time resolved dissipated power density $p_{\mathrm{e,i}}$ directly resulting from the PIC simulation:

$$\bar{p}_{\mathrm{e,i}} = \frac{1}{d \cdot T_{\mathrm{lf}}} \int_0^{T_{\mathrm{lf}}} \int_0^{d} p_{\mathrm{e,i}}\, dx\, dt \tag{22}$$

Here T_{lf} is the duration of one 1 ω RF period and d is the electrode gap. The result for the total dissipated power as well as the electron and ion components are shown in figure 12. The absorbed power density is essentially constant and does not differ from its mean value by more than about 6%. This means, that keeping the applied voltage amplitude constant in the simulation corresponds to a good approximation to keeping the power constant. The small

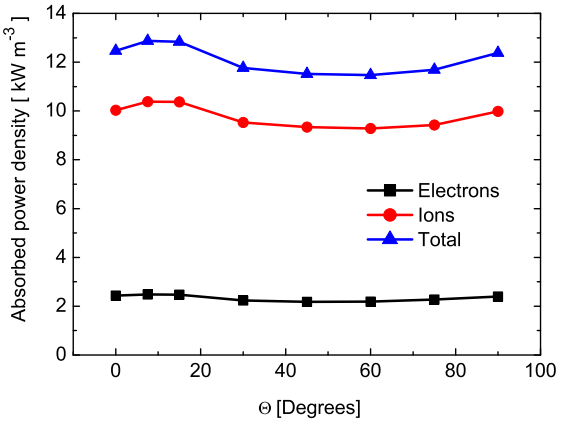

Figure 12. Power absorbed by electrons and ions and total power absorbed as a function of the phase angle θ (PIC) [49].

modulations of the absorbed power reflect the small modulations of the ion flux (figure 11). Therefore, the ion flux might change even less, if the power is kept constant.

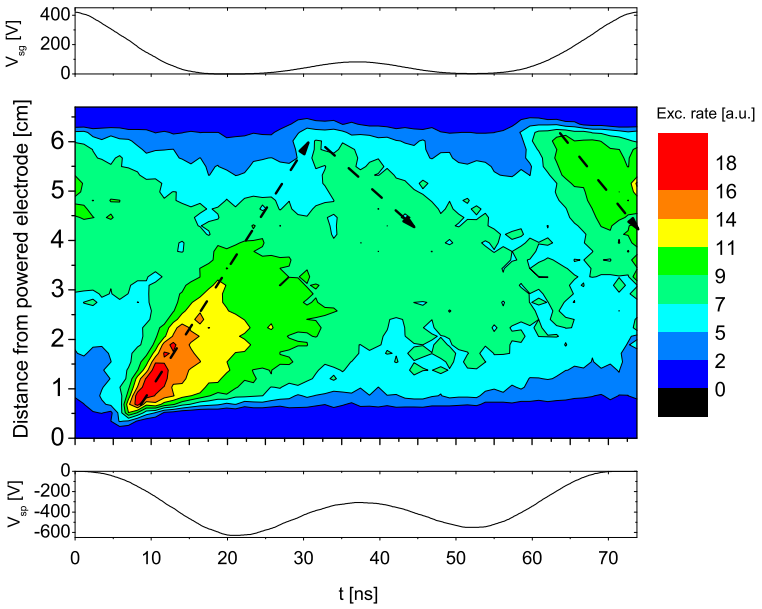

Figure 13. Spatio-temporal plot of the total excitation rate of argon atoms at $\Theta = 7.5°$ calculated by the PIC simulation. The voltages across the sheath at the powered electrode, V_{sp}, and across the sheath at the grounded electrode, V_{sg}, are also shown [49].

The spatio-temporal total excitation rate of argon atoms at $\Theta = 7.5°$ (phase of strongest DC

self bias) is shown in figure 13. The generation of beams of highly energetic electrons by the expanding sheath at both electrodes is observed. Such electron beams have been investigated experimentally and theoretically before [16, 18, 19, 20, 21, 22, 24, 25, 42, 44, 47, 49]. As the discharge is asymmetric at this phase angle (see figure 4), the sheath width and sheath expansion velocities are different at each electrode. Therefore [2, 3], the observed electron beams at each electrode are different. The strongest excitation is caused by the initial sheath expansion of the sheath at the powered electrode.

5. Conclusions

The Electrical Asymmetry Effect - a novel and simple method to achieve efficient separate control of ion energy and ion flux at the electrodes in capacitively coupled radio frequency discharges - has been discovered. If a temporally symmetric voltage waveform is applied to a capacitively coupled radio frequency (CCRF) discharge, that contains one or more even harmonics of the fundamental frequency, the sheaths in front of the two electrodes will necessarily be asymmetric even in a geometrically symmetric discharge. The EAE was analyzed by an analytical model, a fluid/Monte Carlo model and a PIC simulation.

The analytical model showed that a DC self bias is generated even in a geometrically symmetric discharge if the extremes of the applied RF voltage waveform are different. If a fundamental frequency and its second harmonic are applied to one electrode, the symmetry of the applied voltage waveform can be changed by adjusting the phase angle between the applied voltage harmonics. Consequently, the DC self bias can be controlled by simply changing the phase and the role of both electrodes (powered and grounded) can be reversed.

The fluid/Monte Carlo model demonstrated that this variable DC self bias provides a unique opportunity to control the IEDF at both electrodes via the phase angle. It also showed that the mean ion densities in both sheaths are different at low pressures and at phase angles of non-vanishing DC self bias due to flux continuity. Therefore, the symmetry parameter deviates from unity and the EAE is self-amplifying.

A self consistent PIC simulation finally showed that the EAE allows efficient separate control of ion energy and flux at the electrode surfaces. The ion flux is found to be constant within $\pm 5\,\%$ when changing the phase angle, while the maximum ion energy is changed by a factor of about three. This result is particularly interesting for industrial applications, since it allows efficient separate control of ion flux and energy using an easily applied technique. In many cases existing process chambers could be easily modified to make use of the EAE by simply replacing the matching and power supply. Using this technique reactor sizes and, consequently, costs can be reduced, since high area ratios are no longer needed. Furthermore, limitations of the separate control of ion flux and energy by the frequency coupling in conventional dual-frequency CCRF discharges operated at substantially different frequencies can be avoided.

A method for controlling the ion energy based upon this effect is patent pending (PCT application No PCT/EP2008/059133).

Acknowledgements

This work has been funded by the DFG through GRK 1051, the Ruhr University Research School and the Hungarian Scientific Research Fund through grants OTKA-T-48389 and OTKA-IN-69892.

References

[1] Lieberman M A and Lichtenberg A J 2005, Principles of Plasma Discharges and Materials Processing, 2nd. ed., Wiley Interscience, NJ: Wiley
[2] Lieberman M A 1988 *IEEE Trans. on Plasma Sci.* **16** No. 6 638
[3] Lieberman M A and Godyak V A 1998 *IEEE Trans. on Plasma Sci.* **26** 955
[4] Surendra M and Graves D B 1991 *Phys. Rev. Lett.* **66** 1469
[5] Turner M M 1995 *Phys. Rev. Lett.* **75** 1312
[6] Gozadinos G, Turner M M and Vender D 1995 *Phys. Rev. Lett.* **87** 135004
[7] Kaganovich I D 2002 *Phys. Rev. Lett.* **89** 265006
[8] Kaganovich I D, Polomarov O V and Theodosioue C E 2006 *IEEE Trans. on Plasma Sci.* **34** No. 3 696
[9] Klick M 1996 *J. Appl. Phys.* **79** 3445
[10] Klick M, Kammeyer M, Rehak W, Kasper W, Awakowicz P and Franz G 1998 *Surf. Coat. Technol.* **98** 1395
[11] Mussenbrock T and Brinkmann R P 2006 *Appl. Phys. Lett.* **88** 151503
[12] Mussenbrock T and Brinkmann R P 2007 *Plasma Sources Sci. Technol.* **16** 377-385

[13] Czarnetzki U, Mussenbrock T and Brinkmann R P 2006 *Phys. Plasmas* **13** 123503
[14] Lieberman M A, Lichtenberg A J, Kawamura E, Mussenbrock T and Brinkmann R P 2008 *Phys. Plasmas* **15** 063505
[15] Mussenbrock T, Brinkmann R P, Lieberman M A, Lichtenberg A J and Kawamura E, 2008 *Phys. Rev. Letters* **101** 085004
[16] Donkó Z, Schulze J, Luggenhölscher D, and Czarnetzki U 2008 submitted to Phys. Rev. Letters
[17] Ziegler D, Mussenbrock T and Brinkmann R P 2008 *Plasma Sources Sci. Technol.* **17** 045011
[18] Schulze J, Heil B G, Luggenhölscher D, Mussenbrock T, Brinkmann R P and Czarnetzki U 2008 *J. Phys. D FTC* **41** 042003
[19] Schulze J, Heil B G, Luggenhölscher D, Brinkmann R P and Czarnetzki U 2008 *J. Phys. D* **41** 195212
[20] Schulze J, Donkó Z, Heil B G, Luggenhölscher D, Mussenbrock T, Brinkmann R P and Czarnetzki U 2008 *J. Phys. D* **41** 105214
[21] Schulze J, Kampschulte T, Luggenhölscher D and Czarnetzki U 2007 *IOP Conf. Series* **86** 012010
[22] Schulze J, Heil B G, Luggenhölscher D and Czarnetzki U 2008 *IEEE Trans. on Plasma Sci.* **36** 1400
[23] Salabas A, Marques L, Jolly J and Alves L L 2004 *J. Appl. Phys.* **95** 9 4605-4620
[24] Vender D and Boswell R W 1990 *IEEE Trans. Plasma Sc.* **18** 725
[25] Wood B P 1991 *PhD thesis* University of California at Berkely
[26] Tochikubo F, Suzuki A, Kakuta S, Terazono Y and Makabe T 1990 *J. Appl. Phys.* **68** 11 5532
[27] Petrović Z Lj, Tochikubo F, Kakuta S, and Makabe T 1992 *J. Appl. Phys.* **71** 2143
[28] Czarnetzki U, Luggenhölscher D and Döbele H F 1999 *Plasma Sources Sci. Technol.* **8** 230
[29] Gans T, Schulz-von der Gathen V and Döbele H F 2004 *Europhysics Letters* **66** 232
[30] Belenguer Ph, and Boeuf J P 1990 *Phys. Rev. A* **41** 4447
[31] Sato A H and Lieberman M A 1990 *J. Appl. Phys.* **68** 12 6117
[32] Vender D and Boswell R W 1992 *J. Vac. Sci. Technol. A* **10** 4 1331
[33] Turner M M and Hopkins M B 1992 *Phys. Rev. Letters* **69** 24 3511
[34] Rauf S and Kushner M J 1999 *IEEE Trans. on Plasma Science* **27** 1329
[35] Boyle P C , Ellingboe A R and Turner M M 2004 *Plasma Sources Sci. Technol.* **13** 493-503
[36] Boyle P C, Ellingboe A R and Turner M M 2004 *J. Phys. D.* **37** 697
[37] Kitajima T, Takeo Y, Petrovic Z L and Makabe T 2000 *Appl. Phys. Lett.* **77** 489
[38] Denda T, Miyoshi Y, Komukai Y, Goto T, Petrovic Z L and Makabe T 2004 *J. Appl. Phys.* **95** 870
[39] Lee J K, Manuilenko O V, Babaeva N Yu, Kim H C and Shon J W 2005 *Plasma Sources Sci. Technol.* **14** 89
[40] Kawamura E, Lieberman M A and Lichtenberg A J 2006 *Phys. Plasmas* **13** 053506
[41] Turner M M and Chabert P 2006 *Phys. Rev. Lett.* **96** 205001
[42] Gans T, Schulze J, O'Connell D, Czarnetzki U, Faulkner R, Ellingboe A R and Turner M M 2006 *Appl. Phys. Lett.* **89** 261502
[43] Schulze J, Gans T, O'Connell D, Czarnetzki U, Ellingboe A R and Turner M M 2007 *J. Phys. D* **40** 7008-7018
[44] Schulze J, Donkó Z, Luggenhölscher D and Czarnetzki U 2009 *Plasma Sources Sci. Technol.* in print
[45] Semmler E, Awakowicz P and von Keudell A 2007 *Plasma Sources Sci. Technol.* **16** 839
[46] Salabas A and Brinkmann R P 2005 *Plasma Sources Sci. Technol.* **14** 2 53-59
[47] Heil B G, Schulze J, Mussenbrock T, Brinkmann R P and Czarnetzki U 2008 *IEEE Trans. on Plasma Sci.* **36** 1404
[48] Heil B G, Czarnetzki U, Brinkmann R P and Mussenbrock T, 2008 *J. Phys. D* **41** 165202
[49] Donkó Z, Schulze J, Heil B G, Czarnetzki U 2009 *J. Phys. D* **42** 025205
[50] Heil B G, Brinkmann R P and Czarnetzki 2008 *J. Phys. D* **41** 225208
[51] Godyak V A, Piejak R B and Alexandrovich B M 1992 *Plasma Sourc. Sci. Technol.* **1** 36
[52] Kratzer M, Brinkmann R P, Sabisch W and Schmidt H 2001 *J. Appl. Phys.* **90** 2169
[53] Brinkmann R P 2007 *J. Appl. Phys.* **102** 093302
[54] Donkó Z and Petrović Z 2006 *Japanese Journal of Applied Physics* **45** 8151
[55] Donkó Z and Petrović Z 2007 *J. Phys.: Conf. Series* **86** 012011
[56] Phelps A V, Petrović Z Lj 1999 *Plasma Sources Sci. Technol.* **8** R21
[57] Phelps A V 1994 *J. Appl. Phys.* **76** 747
[58] Phelps A V, *http://jilawww.colorado.edu/˜avp/collision_data/* unpublished
[59] Tsuboi H, Itoh M, Tanabe M, Hayashi T and Uchida T 1995 *Jpn. J. Appl. Phys.* **34** 2476
[60] Chinzei Y, Ogata M, Sunada T, Itoh M, Hayashi T, Shindo H, Itatani R, Ichiki T and Horiike Y 1999 *Jpn. J. Appl. Phys.* **37** 4572